IOP Conf. Series: Journal of Physics: Conf. Series **830** (2017) 012151 doi:10.1088/1742-6596/830/1/012151

Trace-transform invariants of tracks of high-velocity jets from the surface of tungsten droplets in the plasma flow

P Gulyaev[1], V Jordan[2,3], I Gulyaev[1,3], A Dolmatov[1]

[1] Physics and Chemistry Department, Ugra State University, 16 Chekhov street, Khanty-Mansiysk, 628012, Russian Federation
[2] Physics Department, Altai State University, 61 Lenin avenue, Barnaul, 656049, Russian Federation
[3] Laboratory for plasma dynamics of disperse systems, Khristianovich Institute of theoretical and applied mechanics Siberian branch of Russian Academy of Sciences, 4/1 Institutskaya street, Novosibirsk, 630090, Russian Federation

E-mail: p_gulyaev@ugrasu.ru

Abstract. The paper presents the analysis of the recorded tracks of high-velocity emission in the air-argon plasma flow during breaking up of tungsten microdroplets. This new physical effect of optical emission involves two stages. The first one includes thermionic emission of electrons from the surface of the melted tungsten droplet of 100–200 μm size and formation of the charged sphere of 3–5 mm diameter. After it reaches the breakdown electric potential, it collapses and produces a spherical shock wave and luminous radiation. The second stage includes previously unknown physical phenomenon of narrowly directed energy jet with velocity exceeding 4000 m/s from the surface of the tungsten droplet. The luminous spherical collapse and high-velocity jets were recorded using CMOS photo-array operating in a global shutter charge storage mode. Special features of the CMOS array scanning algorithm affect formation of distinctive signs of the recorded tracks, which stay invariant to trace transform (TT) with specific functional. The series of concentric circles were adopted as primitive object models (patterns) used in TT at the spherical collapse stage and linear segment of fixed thickness – at the high-velocity emission stage. The two invariants of the physical object, motion velocity and optical brightness distribution in the motion front, were adopted as desired identification features of tracks. The analytical expressions of the relation of 2D TT parameters and physical object motion invariants were obtained. The equations for spherical collapse stage correspond to Radon–Nikodym transform.

1. Introduction

This report focuses on the analysis of video frames capturing phenomenon of high-speed photoluminescence in a jet of low-temperature argon plasma [1,2]. We assume that this phenomenon can be attributed to guided ionization waves or "plasma bullets" (PB), which have been intensively investigated in atmospheric-pressure plasma jets in the past decade [3]. The peculiarity of our case is that high-speed emissions arose spontaneously and unpredictably in the process of fragmentation of liquid tungsten microdroplets. At present, the physical mechanism of initiation, evolution and formation of the propagation direction of such emissions is not clear and should be investigated in future work. As far as we know from the recorded video data, these high-speed emissions or PB do not

interfere with each other. The main questions are: what is the nature of these high-speed objects, what factors determine their direction and what is the source of photoluminescence.

Photo-detector arrays (CMOS and CCD) operating in a charge accumulation mode produce specific distortions of images of fast-moving objects. These distortions appear as blurring of the image along the objects motion direction and complicate the analysis of its actual size and velocity. The goal of the present paper is determination of the basic invariants of motion: the velocity and the shape of the high-velocity objects which have to be immutable to variation of the exposure time and spatial resolution of the video camera.

2. Experiment and Equipment

The optical imaging system includes a digital camera HD1-1312 (PhotonFocus AG) with CMOS sensor of 1312*1082 size and photospectrometer LR-T1 (Aseq) with a spectral range of 300–1000 nm [4]. The bandpass filter with a central wavelength of 575 nm (FWHM 50 nm) was installed in the optical channel of the camera, and recording was conducted with a frequency of 55 frames per second. The applied camera lens provided a spatial resolution of 51.9 micrometer/pixel. The focal plane of the optical systems of the camera and photospectrometer were matched, the measurement region of the spectrometer was a circle 10 mm in diameter located in the center of the video camera frame.

Numerous video frames contain images of highly luminescent emission from melted tungsten particles moving in the plasma flow [2]. For example, figure 1 demonstrates the sources of intense radiation 1–2 mm in diameter around tungsten particles. In the same figure, ordinary tracks of tungsten droplets 100 microns in diameter and 0.5–1 mm in length can be seen. Notably, all high-velocity emissions are directed along the local direction of the motion a two-phase jet. The study of the spectrum of the total radiation of the jets (figure 2) showed no appearance of additional lines and bands in the spectral range of 555–595 nm when working with tungsten material compared to steel case. In addition, the spectral pyrometry method [5, 6] was applied to the continuous (thermal) spectrum in the 520–650 nm range which allowed us to find the temperature of the steel droplets in the cross section of 9 cm below the torch nozzle to be 2730–3090 K, and tungsten droplets – 3650–3890 K. The analysis of the video frames shows that plasma radiation in this area is not considerable, so we can assume that the measured temperature corresponds to the hottest particles of the dispersed phase. [7,8].

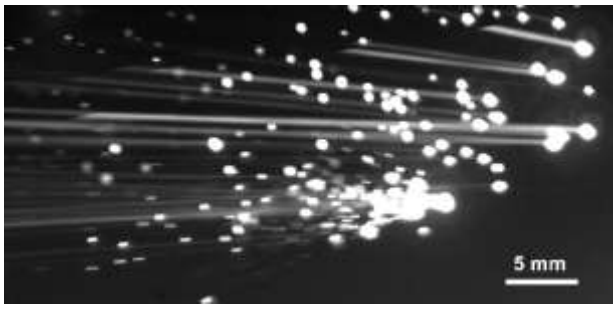

Figure 1. Group of tungsten droplets being a source of high-velocity emissions. Scale 51.9 microns/ pixel, frame exposure time is 10 μs.

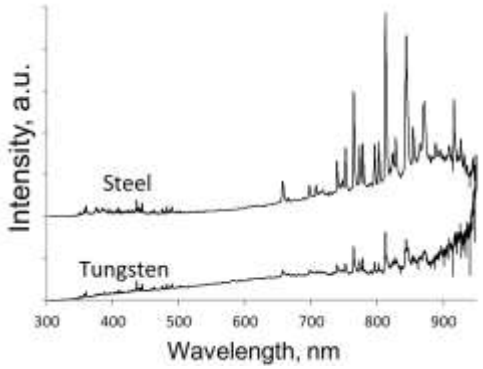

Figure 2. The spectra of emission of two-phase jets 9 cm downstream from the DC plasma torch nozzle when spraying steel (top) and tungsten (bottom) material.

Figure 3 (left) shows the images of several tracks of high-velocity emissions, in particular, the upper track corresponds to figure 4. As can be seen, the width of the tracks of various high-velocity emissions varies between 0.2–1 mm. Figure 3 (right) also shows the brightness distribution along the length of the respective tracks. It is important that the brightness of a track is not uniform along its length, and it has a wave shape. The length of such waves is different between the tracks and belongs

to the 5–15 mm range. Simultaneously, an individual track wavelength increases with increasing distance from the source of emission (particles). In the upper graph of figure 3 one can see a tooth-shaped structure with a period of 1–1.2 mm. A close examination of the middle graph reveals similar structure with 4–5 mm wavelength.

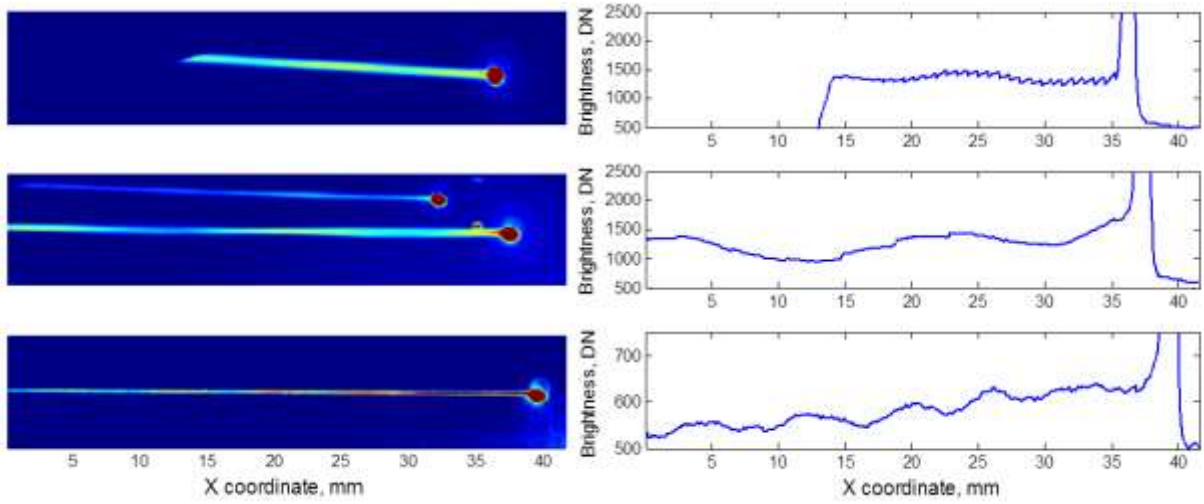

Figure 3. Images of individual tracks of high-speed emissions (left) and luminance distribution graphs along their length (right).

Let us consider a single particle with high-velocity emission in more detail (figure 4). The area in the immediate vicinity of the particle (about 1.5 mm in diameter) is occupied by radiation caused, probably, by the most intense stage of the gas discharge. A series of nearly spherical contours is observed around emitting particles, the diameters of spheres are about 2 mm, 4 mm, 6 mm and 9 mm, the brightness of spheres descends and the center is displaced from the particle to the outer region of the plasma stream (in figure 4 – upward) with diameter increase. The nature of these spheres cannot be attributed to light scattering by the particles of the surrounding atmosphere (such as halo or solar rainbow) since in the considered case the light wavefront is spherical rather than flat.

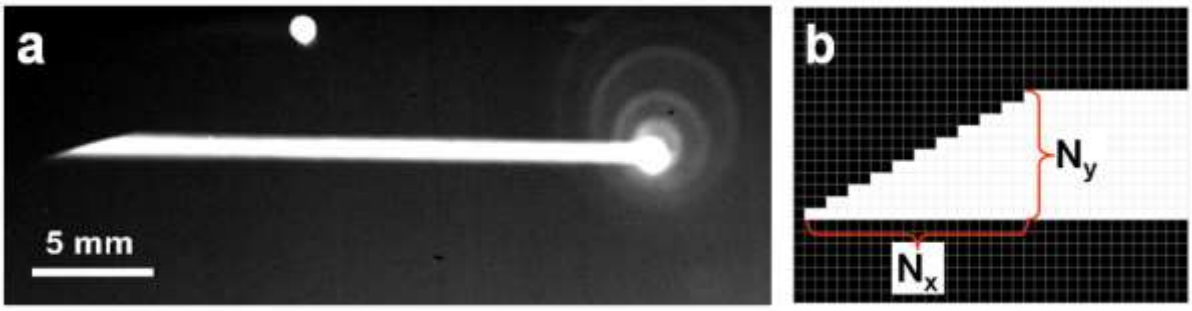

Figure 4. Typical image of a radiating particle and high-velocity emission. The frame exposure time 10 μs (a). Raster image of the tip of the track. For calculation of the propagation velocity of the emission (b).

All the video frames containing the entire (complete) tracks of high-velocity emissions demonstrate that their tips have a linearly cut shape (figure 4). A general analysis of the CMOS sensor operation algorithm provides explanation of this effect. Modern photo-arrays operate in a "global shutter" mode in which the start and end signal (charge) accumulation in the photosensitive region of each array cell takes place simultaneously, after which the charge is moved to a "floating diffusion" region (FD) and consequently is read out with a frequency of the onboard chip [6,7]. Depending on the architecture of CMOS array, accumulation of photo-electrons can occur even at the stage of storage in the FD region.

In fact, the exposure time of cells in adjacent rows will be different, which makes it possible to determine the velocity of the moving object from the slope of its image blurring. The clock frequency of the A1312 sensor (PhotonFocus AG) is 40 MHz, thus, the signal accumulation time differs in adjacent rows by 25 ns. Figure 4, b schematically illustrates a bitmap track tip and designates its length N_x and width N_y (in pixels). The velocity of the moving object can be calculated by the formula $V = (s \cdot N_x)/(\tau \cdot N_y)$ where s is the image scale. The calculation for the track in figure 4, using values $N_x = 52$, $N_x = 17$, s =51.9 microns, $\tau = 25$ ns, gives the value of the velocity V = 6350 m/s. Given that the total length of the track is 22 mm, one can suggest that the frame in figure 4 has been taken 3.5 μs after the emission has taken place. The measurements of other tracks velocity preferably lie in the range of 3–10 km/s, and the maximum value is 20 km/s. It may be noted that the obtained values are in good agreement with the above-obtained conservative estimate of 4.2 km/s.

Figure 5 provides description of three zones of interest for analysis of distortions of moving objects images recorded with CMOS photo-arrays operating in the charge storage mode with a global shutter.

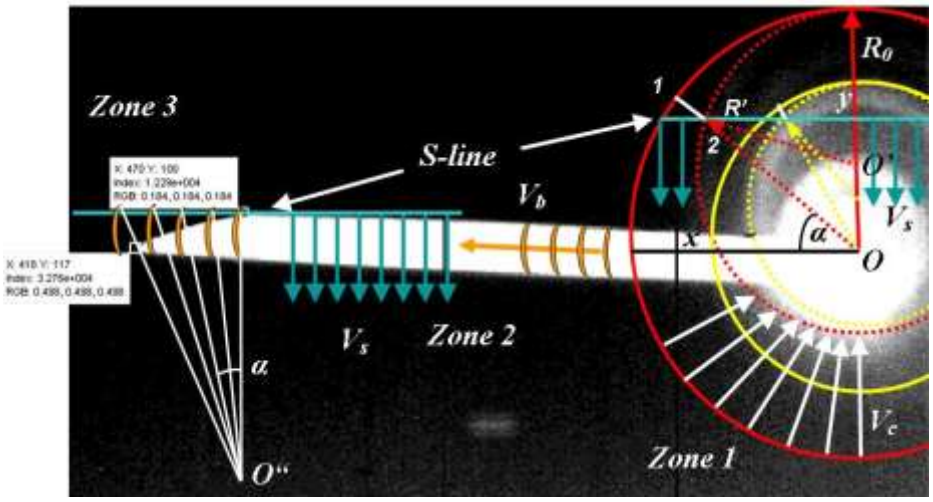

Figure 5. Three zones of interest in trace-transform during recording high-velocity discharge: zone 1 is the collapse and parallax of a spherical shock wave; zone 2 is the translator motion of the high-velocity emission and uniform "blur" of the image (Abel transform); zone 3 is the intersection of the photo-array read out lines and the image of the high-velocity object (Radon transform).

CMOS array scanning algorithm provides formation of distinctive signs of the recorded tracks, which stay invariant to trace transform (TT) with a specific functional. The series of concentric circles were adopted as primitive object models (patterns) used in TT at the spherical collapse stage (zone 1) and a linear segment of fixed thickness – at the high-velocity energy jet stage (zone 2). The two invariants of physical object – motion velocity and optical brightness distribution in the motion front, were adopted as desired identification features of tracks.

The following notation will be used: V_s is vertical speed of scanning lines (S-line) of the photo-array; V_c is radial velocity of a spherical shock-wave collapse; V_b is the velocity of the high-velocity object (plasma bullet); (x, y) are plane coordinates of the intersection of the scanning line (S-line) in the current time moment t. Given that in zone 1 all the luminescence objects are radially symmetric functions $f(x, y) = f(r)$, where r is the radius vector from the coordinate system center O, using the polar coordinates system, we have:

$$\begin{cases} x = r\cos\alpha \\ y = r\sin\alpha \end{cases}.$$

In accordance with figure 5, the coordinates of the image of the first spherical zone collapse can be written as follows:

$$\begin{cases} x = (R_0 - V_c t)\cos\alpha \\ y = R_0 - V_s t \end{cases}.$$

It is easy to calculate the coordinate of the center of a spherical wave image offset, subjected to the TT of Abel-Radon, using the Pythagoras' theorem:

$$y^{|I} = R_0\left(1 - \frac{V_s}{V_s + V_c}\right).$$

Obviously, the subject of non-zero values of the variables t and difference (V_c-V_s), one can determine the value V_c if V_s is known. To do this, one has to calculate the relative displacement of the centers of the two spherical shock waves (figure 4). After that, the expansion velocity is determined by the standard time-of-flight method [9,10]. It should be noted that the vertical displacement of the spherical shock waves centers is possible only if spherical front velocity has opposite signs in upper and lower parts of the zone, i.e. sphere is contracting to the center as shown in figure 5.

3. Basic physical phenomena and theoretical models

As mentioned above, the physical mechanism of the observed phenomenon is not completely clear, however, experimental results allow one to suggest that this is a form of gas discharge followed by directed high-velocity emission of charged particles – electrons. It is clear that realization of gas discharge requires the formation regions with high electric field. Under considered conditions of two-phase plasma flow this can be provided by thermionic emission of electrons from the surface of the metal droplets. As a result, the metal droplet itself acquires a positive charge and an electron cloud around it – negative charge. The reason why this effect was observed only with tungsten droplets is probably the high melting temperature of the material. As is known, thermionic emission current density obeys the Richardson-Dushman law: $j = A \cdot T^2 \cdot \exp(-W/kT)$, where T is the temperature of the material, W is electron work function of material, A is Richardson constant, and k is Boltzmann constant. Figure 6 shows the calculation of the thermionic current density for basic metal materials used in plasma spraying, based on the temperature range corresponding to their liquid state.

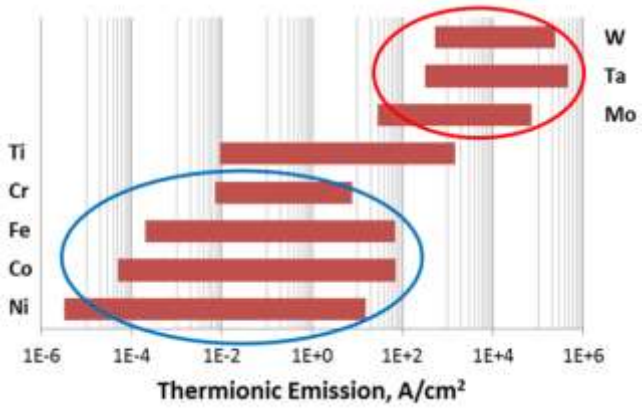

Figure 6. Thermionic current density for basic metals in the temperature range between material melting and boiling points.

The range of j weakly depends on the values of A and W ($A = 30 \div 60$ A·K^{-2}cm^{-2}, W =3.9-4.6 eV for these materials), and it is mainly determined by the material surface temperature. As can be seen, the intensity of thermionic emission of W, Ta and Mo metals group is 2–4 orders of magnitude higher

than that of Cr, Fe, Co, Ni group. Thus, we believe that the appearance of the observed effect is due to the tungsten particle high thermionic emission of electrons at their melting temperature.

4. Conclusion

The analysis of the physical nature of high-velocity emissions should start from definition of the type of the observed moving objects. The drift velocity of the electrons in the plasma discharge depends on the value of the reduced electric field E/N (E is electric field, N is the density of charged particles) and it typically is 2–10 km/s. Obviously, the mobility and the drift velocity of heavy charged particles (ions) under the same conditions is several orders of magnitude lower due to the huge difference in their masses. For this reason, it can be assumed that the observed high-velocity emissions are caused by the motion of electrons.

Consider some of the possible causes of anisotropy of directed emission in a spherical discharge around metal droplets. As already noted, all high-velocity emissions propagate in the direction of gas stream. The gas pressure distribution on the surface of a spherical metal droplet is highly uneven: it has the maximum value in the front point, and the minimum value in the stern. Probably, the concentration of charged particles in the vicinity of the droplet follows uneven gas pressure distribution which leads to formation of the preferred direction of emission. Another explanation, more likely in our opinion, can be a displacement of the electron cloud (negatively charged) with respect to the metal droplet (positively charged) due to external gas flow. Thus, at the moment of a discharge, the center of the electron cloud is shifted downstream from the metal droplet. The result is a "cumulative emission" of electrons away from the surface of the metal droplet. Hydrodynamic analogy of such a scenario may be the collapse of cavitation bubbles near a solid surface or hollow droplets collision with a solid surface [11, 12].

The wave shape of the track brightness distribution (figure 3) requires close study as well. This could be explained by the formation of the "shock diamonds" (Mach disks) similarly to the supersonic gas jet. The sound velocity in the argon-air plasma under atmospheric pressure is about 1.5 km/s, i.e. the motion of the emission is supersonic. However, the formation of a "shock diamonds" requires quasi steady-state gas stream for a sufficient length of time, which is difficult to provide in our experimental conditions. Another possible explanation for the track images with a wave structure can be an effect similar to the wakefield acceleration, spatial separation of charges in the wake of a driver (dense cluster of charged particles or laser pulse) moving at nearly the light-speed. Assume that the temperature of the argon plasma is 3–5 thousand degrees, the ionization degree is approximately 10^{-4}, the density of charged particles is 10^{20} m^{-3}, and the plasma frequency $\omega_p = 10^{11}$ s^{-1}. Considering that in this case, the driver is a bunch of electrons at a speed of $V = 10^4$ m/s, we should expect antinodes in the wake of a size of $\lambda = V/\omega_p \sim 0.1$ μm. However, as we can see in figure 3, the typical wavelength values are 4 orders of magnitude higher – several millimeters. In such case, we have to suggest that the driver velocity should also be near the light-speed.

Acknowledgments

The reported study was funded by RFBR according to the research projects No. 15-42-00106 and No. 15-48-00100.

References

[1] Gulyaev I P, Dolmatov A V, Kharlamov M Yu, Gulyaev P Yu, Jordan V I, Krivtsun I V, Korzhyk V M and Demyanov O I 2015 *Journal of Thermal Spray Technology* **24** 1
[2] Gulyaev I P, Dolmatov A V, Gulyaev P Yu, Iordan V I, Kharlamov M Yu and Krivtsun I V 2016 *IOP Conference Series: Materials Science and Engineering* **110** 012057
[3] Lua X, Naidisb G V, Laroussic M and Ostrikov K 2014 *Physics Reports* **540** 123
[4] Dolmatov A V, Gulyaev I P and Jordan V I 2015 *IOP Conference Series: Materials Science and Engineering* **81** 012041

[5] Dolmatov A V, Gulyaev I P, Gulyaev P Yu and Iordan V I 2016 *IOP Conference Series: Materials Science and Engineering* **110** 012058
[6] Boronenko M P, Seregin A E, Gulyaev P Yu and Milyukova I V 2015 *Scientific Visualization* **7** 102
[7] Boronenko M P, Gulyaev P Yu, Seregin A E and Bebiya A G 2015 *IOP Conference Series: Materials Science and Engineering* 2015 **93** 012021
[8] Boronenko M P, Gulyaev P Yu, Seregin A E and Poluhina K G 2015 *Journal of Physics: Conference Series* 2015 **643** 012028
[9] Garkol' D A, Gulyaev P Y, Evstigneev V V and Mukhachev A B 1994 *Combustion, Explosion, and Shock Waves* **30** 72
[10] Gulyaev P Yu, Cui H Z, Gulyaev I P and Milyukova I V 2015 *High Temperatures - High Pressures* **44** 83
[11] Gulyaev I P, Solonenko O P, Gulyaev P Yu and Smirnov A V 2009 *Technical Physics Letters* **35** 885
[12] Gulyaev I P and Solonenko O P 2013 *Experiments in Fluids* **54** 1432